



SELF-CONSISTENT MODELLING OF THE PLASTIC DEFORMATION OF F.C.C. POLYCRYSTALS AND ITS IMPLICATIONS FOR DIFFRACTION MEASUREMENTS OF INTERNAL STRESSES

B. CLAUSEN^{1,2}, T. LORENTZEN¹ and T. LEFFERS¹

¹Materials Research Department, Risø National Laboratory, 4000 Roskilde, and ²Department of Solid Mechanics, Technical University of Denmark, 2800 Lyngby, Denmark

(Received 30 July 1997; accepted in revised form 12 December 1997)

Abstract—Using a self consistent scheme we model the development of elastic lattice strains during uniaxial loading for selected families of grains with specific orientations. These lattice strains vary dramatically for the different grain orientations, and most families of grains show a high degree of non-linearity at the start of the plastic regime. The 311 reflection does, however, respond almost linearly to loading, and therefore it constitutes a suitable reflection for characterization of macroscopic stresses and strains by diffraction for the given conditions. As a consequence of the high degree of non-linearity in the lattice strain response during loading highly anisotropic intergranular residual lattice strains develop during unloading. The evaluation of the model predictions by neutron diffraction is exemplified by selected results from *in-situ* loading experiments performed on austenitic stainless steel specimens. As a necessary condition for the proper understanding of the results we have included a description of the slip pattern resulting from the model applied and its relation to the slip patterns derived from the upper-bound Taylor model and the lower-bound Sachs model. © 1998 Acta Metallurgica Inc.

1. INTRODUCTION

The measurement of macroscopic residual stresses/internal stresses (type-1 stresses [1]) by diffraction methods is based on the measurement of deviations in lattice spacing for specific crystallographic planes (deviations from the lattice spacing in stress-free material). In the elastic regime there is a linear relation between the macroscopic stress and the deviation in lattice spacing. However, due to the elastic anisotropy in most metals, this linear relation depends on the lattice plane, and we observe large differences in the stress/strain levels between different families of grains with different lattice orientations (leading to intergranular stresses or type-2 stresses [1]). In the plastic regime the orientation dependence is more complicated and the relation between macroscopic stress and the deviation in lattice spacing becomes highly non-linear.

In simple polycrystal deformation models such as the Sachs [2], the Taylor [3] and the Bishop-Hill models [4–6] elastic anisotropy plays no role. The more sophisticated self-consistent models, see [7–10], includes the elastic anisotropy and they are therefore attractive modeling schemes when the focus is on the effect of elastic (and plastic) anisotropy on the generation of elastic lattice strains. We have selected Hutchinson's self-consistent model [7] which is implemented as described in detail in [11].

In the present work we calculate the deviations in lattice spacing or the lattice strains for a number of

lattice planes perpendicular to and parallel to the tensile axis for uniaxially loaded aluminum, copper and austenitic stainless steel. The results are relevant for lattice strain measurements by diffraction methods in general, but they are viewed with particular reference to neutron diffraction measurements, which monitor bulk strains as opposed to conventional X-ray measurements of the strains in thin surface layers. As outlined above, the basic aim of this work is to provide a rational theoretical background for measurements of the macroscopic stress, for type-1 stress measurements. The results to be presented may, however, also be used for experimental evaluation of the polycrystal model by comparison with diffraction measurements on specimens subjected to macroscopically uniform tensile stresses (during loading and after unloading), and selected experimental results will be quoted. Experimental evaluation of the numerical model is exemplified in [12].

Kröner's original self-consistent polycrystal model [8] (with purely elastic interaction with the continuum matrix) leads to a slip pattern which, after the elastic-plastic transition, is almost identical to the well-known slip pattern of the upper-bound Taylor model. Hutchinson's model (with elastic-plastic interaction with the continuum matrix) leads to a rather different slip pattern which has never been described in details in open literature. This slip pattern is essential for the proper

understanding of the lattice strain calculation. After the description of the present implementation of Hutchinson's model in Section 2 we therefore, as Section 3, include a description of the resulting slip pattern and its relation to the slip pattern derived from the upper-bound Taylor model and the lower-bound Sachs model.

In the present work we consider three f.c.c. materials: aluminum, copper and austenitic stainless steel. They stand for different degrees of elastic anisotropy, which is a parameter of great importance in diffraction measurements of residual and internal stresses.

2. MODEL DESCRIPTION

Hutchinson's model is a rate-insensitive incremental self-consistent model with $\{111\}\{110\}$ slip as the mechanism for plastic deformation. The self-consistent scheme includes the elastic-plastic interaction between the grains which are regarded as spherical inclusions in an infinite homogeneous matrix with the overall *effective* polycrystal moduli. The model is restricted to low strains as the strain definition does not include second order terms or instabilities such as necking.

The controlling parameters for slip are the critical resolved shear stress and the hardening law. The initial critical resolved shear stress, τ_0 , is the same on the 12 slip systems. The current critical resolved shear stress for the i th slip system is denoted τ^i . Its rate of increase is assumed (Hill [13]) to be related to the shear rates, $\dot{\gamma}$, by

$$\dot{\tau}^i = \sum_j h^{ij} \dot{\gamma}^j \quad \text{with } h^{ij} = h_{\gamma} (q + (1-q)\delta^{ij}) \quad (1)$$

where δ^{ij} is Kronecker's delta and the summation is over all active slip systems. The factor q determines the degree of latent hardening: $q = 0$ provides only self hardening, $q = 1$ provides Taylor hardening, and $q > 1$ provides stronger latent hardening than self hardening. The instantaneous hardening coefficient, h_{γ} , depends on the previous deformation history. In the present implementation of the model, the relation between the accumulated slip, γ^{acc} , and the instantaneous hardening coefficient is described by an exponentially decreasing function

$$h_{\gamma} = h_{\text{final}} (1 + (h_{\text{ratio}} - 1) e^{-h_{\text{exp}} \gamma^{\text{acc}}}) \quad (2)$$

where h_{final} is the final hardening coefficient, h_{ratio} is the ratio between the initial and the final hardening

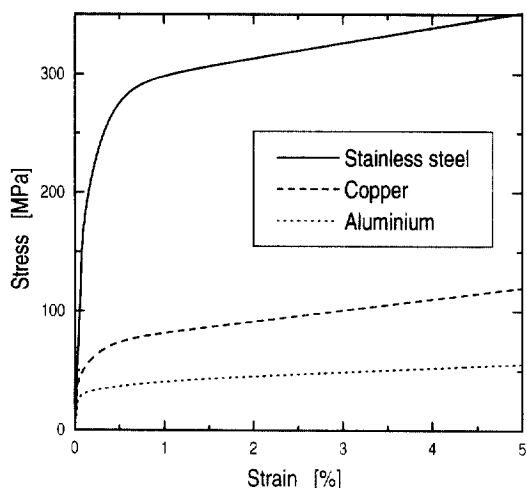


Fig. 1. The calculated stress-strain curves for the selected materials.

coefficient, and h_{exp} is a parameter determining the strength of the exponential part. This formulation includes the simple linear hardening law by selecting $h_{\text{ratio}} = 1$ which reduces equation (2) to $h_{\gamma} = h_{\text{final}}$.

Selection of τ_0 and the hardening coefficients is not trivial. We assume that τ_0 is equal to one half of the largest principal stress difference at yield, where yield is defined as the point where the first grain becomes plastic, a point which is, however, difficult to determine from a stress-strain curve.

In the present calculations, τ_0 and the hardening coefficients (h_{final} , h_{ratio} and h_{exp}) are used as fitting parameters to make the macroscopic stress-strain response of the model resemble the actual macroscopic behavior of the materials. The calculated macroscopic stress-strain response for the three materials is shown in Fig. 1.

The fitting parameters used in the present calculations are listed in Table 1 together with the single crystal stiffness. Taylor hardening ($q = 1$) is avoided, as it causes numerical problems in the slip rate calculation, where the equations to be solved are no longer independent (the well known Taylor ambiguity problem).

The single crystal stiffness quoted for stainless steel actually refer to a FeCrNi alloy whereas the fitting parameters refers to tensile data for a commercially available stainless steel. The compositions are given in Table 2.

In the present calculations the initial orientation distribution is represented by a set of 5000 grains with random texture where the lattice orientations

Table 1. Single crystal stiffness [14, 15] fitting parameters for the three materials

	C_{11} (GPa)	C_{12} (GPa)	C_{44} (GPa)	$2C_{44}/C_{11} - C_{12}$	τ_0 (MPa)	q^a	h_{final} (MPa)	h_{ratio}	h_{exp}
Aluminum	108.2	61.3	28.5	1.22	10.9	1.01	40.0	5.0	61.0
Copper	168.4	121.4	75.4	3.21	15.0	1.01	120.0	17.0	200.0
Stainless steel	204.6	137.7	126.2	3.77	87.0	1.01	140.0	50.0	205.0

^aIt should be underlined that the marginal latent hardening implied in the q value of 1.01 is nothing but a mathematical trick to avoid ambiguity.

Table 2. Chemical composition in wt% for the stainless steel polycrystal as well as for the FeCrNi single crystal

	Cr	Ni	Mo	Mn	Si	C
Single crystal [15]	19.0	10.0	—	—	—	—
Polycrystal	18.25	13.42	3.66	1.48	0.44	0.02

of each grain is described by its three Euler angles, φ_1 , Φ and φ_2 [16]. The lattice rotations during plastic deformation are included even though they are rather small for the low strains dealt with. The relatively high number of grains is necessary because the responses of selected grain sub-sets are to be considered in the investigation of intergranular strain differences in Section 4.

3. THE SLIP PATTERN

In the following we describe various polycrystal deformation parameters related to the slip pattern and their development with strain, concentrating on parameters that relate directly to the crystallographic slip. In particular, we focus on the elastic anisotropy and its bearing on polycrystal deformation in the elastic-plastic transition range and in the fully plastic regime.

In the present model the number of active slip systems in the grains is determined by the stress state in the grain. In the Taylor model, which is based on the assumption that all grains experience the same strain, the number of active slip systems will normally be five so as to accommodate the five independent strain components. In the Sachs model, which is based on the assumption that the stress state in all the grains is the same, only the grains which are oriented along symmetry lines

have more than one active slip system. Neither the Taylor model nor the Sachs model consider the elastic anisotropy of the material.

The number of active slip systems in a grain, as calculated with the present model, varies according to strain and grain orientation. In Fig. 2 the percentages of grains with a given number of active slip systems are shown for aluminum and copper polycrystals as a function of the macroscopic strain. Initially, only one slip system is active. Then another system follows as it appears from the large percentage of grains with two active slip systems after the onset of yield. After 0.5% strain approximately 50% of the grains have three active slip systems, and approximately 30% of the grains have four active slip systems. The difference between the two materials is quite small.

The average number of active slip systems is ~ 3.4 at 0.5% strain, and it increases to ~ 3.6 at 5% strain, which is the highest strain considered. Thus, the number of active slip systems is about halfway between the single slip system in the Sachs model and the five (or more) in the Taylor model.

The orientation dependence of the number of active slip system in the grains of an aluminum polycrystal is shown in Fig. 3 for plastic strain of 0.1% and 1%. At the $\langle 110 \rangle$ orientation the grains have four active slip systems, at the $\langle 111 \rangle$ orientation the grains have up to six active slip systems, and at the $\langle 100 \rangle$ orientation the grains have up to eight active slip systems. This is in agreement with the two-, three- and four-fold symmetries in the cubic lattice. As for the numbers of active slip systems, the orientation distribution of the number of active slip systems are found to be essentially identi-

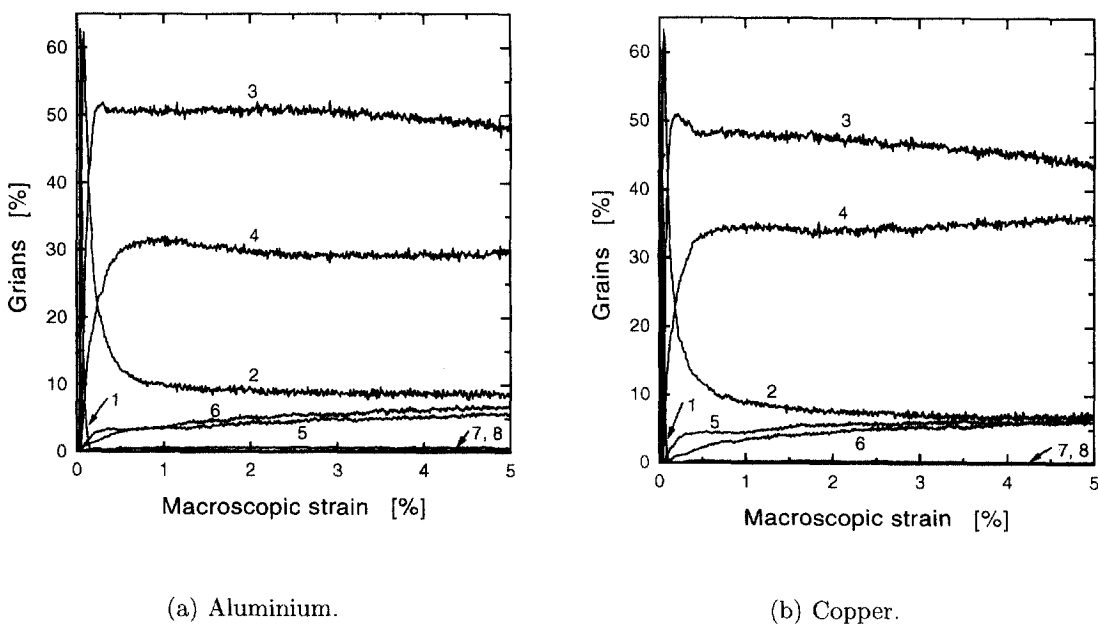


Fig. 2. The number of active slip systems as a function of plastic strain.

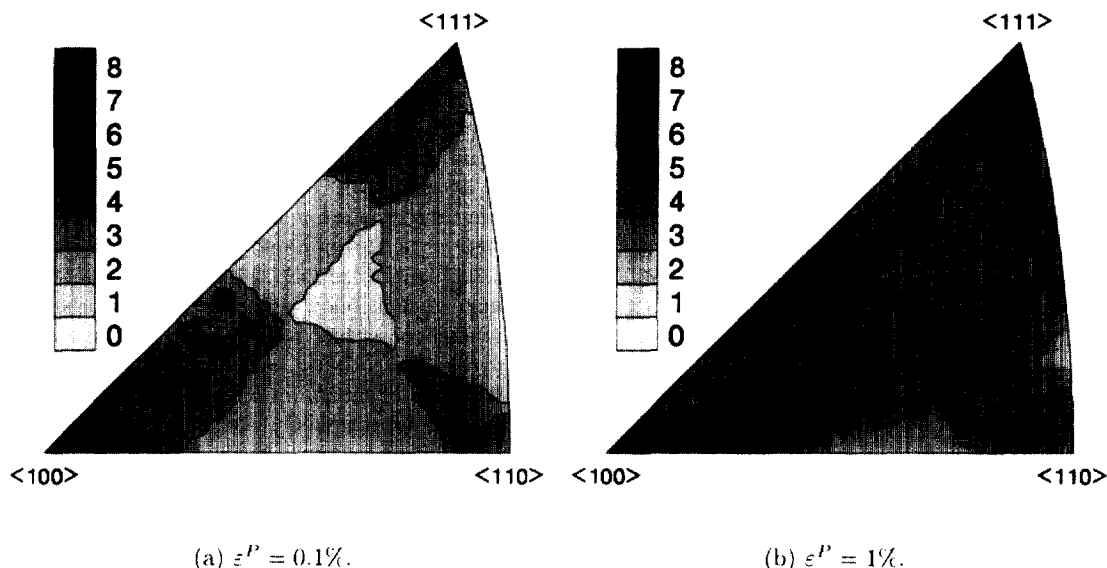


Fig. 3. The number of active slip systems in aluminum as a function of orientation at $\varepsilon^P = 0.1\%$ and at $\varepsilon^P = 1\%$.

cal for aluminum and copper at the plastic strain levels of considered (apart from the very early stage of plasticity, to be described later).

The m -factor (often referred to as the Taylor factor) reflects the total slip activity in the individual grains. It is equal to $\Sigma \dot{\gamma}_i^P / \dot{\varepsilon}^P$ ($\dot{\varepsilon}^P$ being the plastic strain rate in the grain). The average m -factor starts at two at the onset of plastic deformation, and it then increases to an approximately stable value of ~ 2.6 — about halfway between the values of 2.23 and 3.06 for the Sachs and Taylor models, respectively.

The orientation dependence of the m -factor at 0.5% plastic strain in an aluminum polycrystal is shown in the inverse pole figure in Fig. 4(a). The orientation dependence for copper is practically identical to that in Fig. 4(a). For comparison the orientation distribution of the m -factor for the Taylor and the Sachs models is shown in Fig. 4(b),

(c). The results for the present model are clearly closest to the Sachs model. This is particularly clear for orientations close to (110) . In the Sachs model only the four “ideally oriented” slip systems (with identical m -factor of 2.45) are activated. In the Taylor model an additional, “non-ideally oriented”, slip system must be activated, which brings the m -factor up to 3.67. Obviously only the ideally oriented slip systems are activated in the present model.

Thus, independent of elastic anisotropy and strength parameters, the model leads to one “universal” slip pattern about halfway between the slip patterns of the Sachs and Taylor models. One should notice that this universal slip pattern only refers to texture-free f.c.c. materials (or approximately texture-free since the model includes the formation of a weak fiber texture). The slip pattern derived from the model does depend on the texture

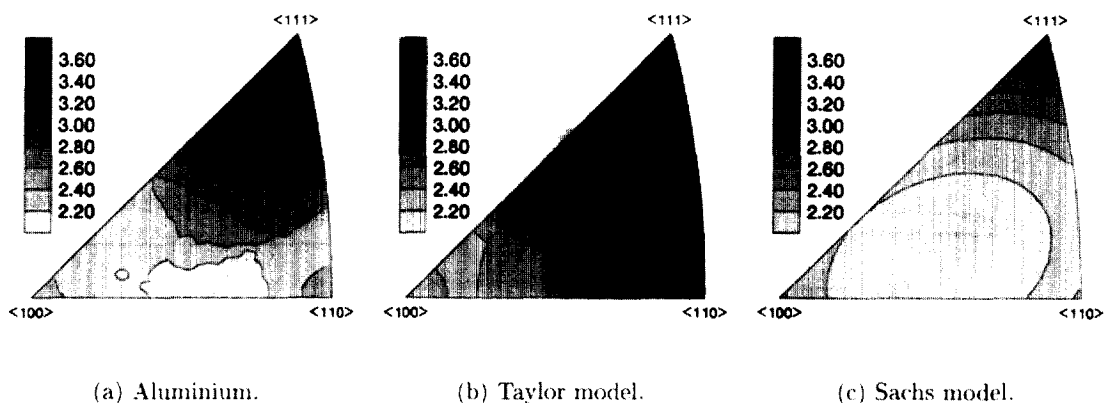


Fig. 4. The m -factor as a function of orientation.

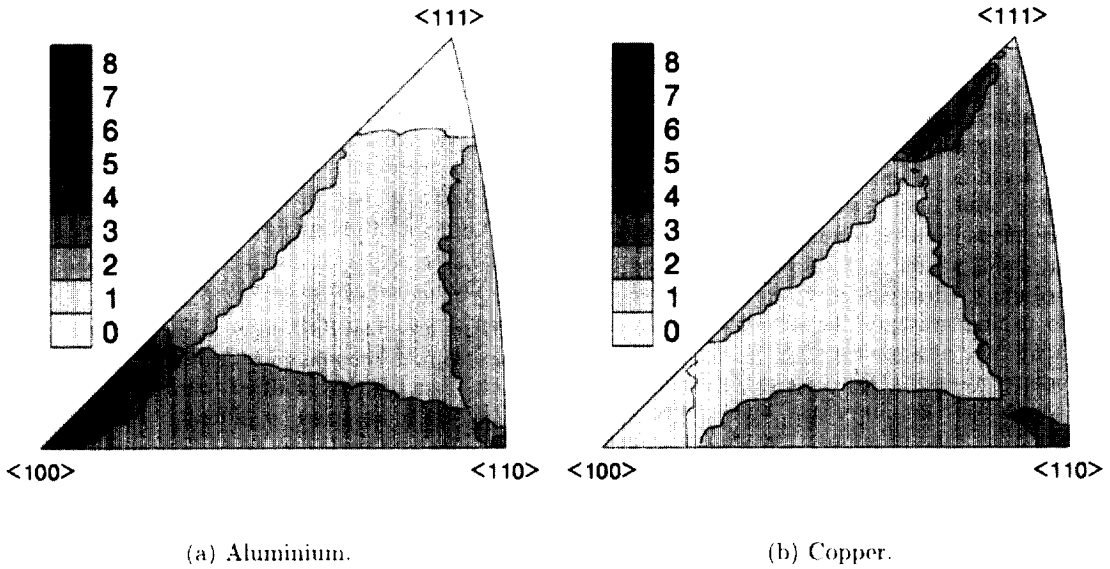


Fig. 5. The number of active slip systems as a function of orientation in aluminum and copper at $\epsilon^P = 0.011\%$.

(not only the average m -factor as in the simpler Sachs and Taylor models, but the whole slip pattern) because the properties of the continuum matrix depends on the texture.

At the very early stage of plastic deformation there is, as one would expect, a clear effect of anisotropy as demonstrated in Fig. 5, which shows the orientation dependence of the number of active slip systems for aluminum and copper at 0.011% plastic strain. In aluminum, without pronounced elastic anisotropy and hence without pronounced stress repartition in the elastic regime, slip has started in the regions next to $\langle 100 \rangle$ and $\langle 110 \rangle$ with the same high Schmid factor and not next to $\langle 111 \rangle$ with a

low Schmid factor. In copper, with its rather high elastic anisotropy, there is stress repartition in the elastic regime: load is transferred from the region next to $\langle 100 \rangle$ to the region next to $\langle 111 \rangle$ (e.g. Figure 6(b)). The result is that slip has started next to $\langle 111 \rangle$ and $\langle 110 \rangle$, whereas slip has not started next to $\langle 100 \rangle$ — with a Schmid factor much higher than that for $\langle 111 \rangle$ and equal to that for $\langle 110 \rangle$. Evidently, the subsequent slip processes soon remove this initial effect of elastic anisotropy.

A more comprehensive description of the slip pattern, including the deformation-induced changes in lattice orientations, is presented in [17].

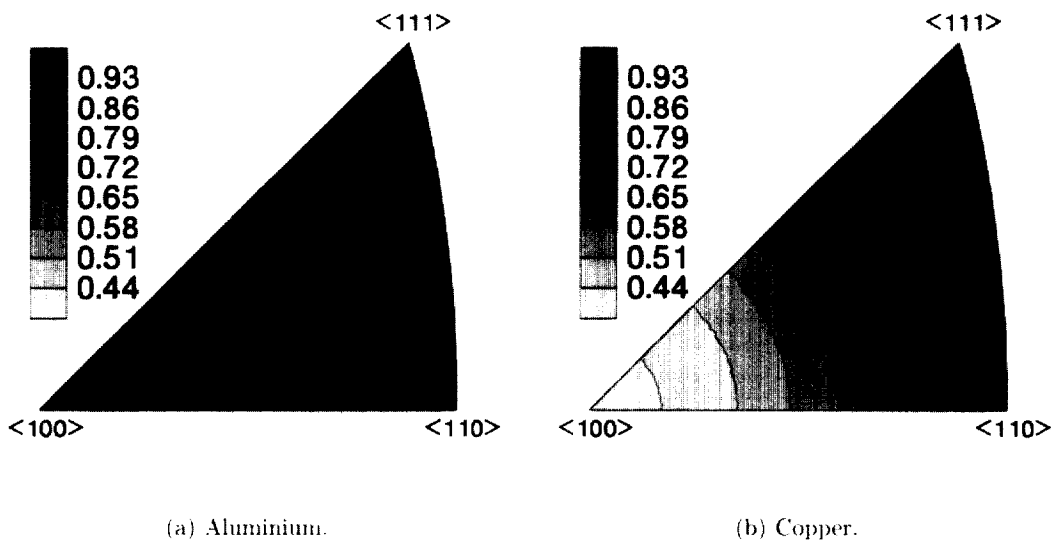


Fig. 6. The normalized effective Young's modulus as a function of crystallographic orientation.

4. LATTICE STRAIN CALCULATIONS

The lattice strains are derived from the model calculations described above: tensile deformation of initially texture-free "samples" of aluminum, copper and stainless steel with 5000 grains. The input parameters for the three materials (aluminum, copper and austenitic stainless steel) were presented in Table 1, and Fig. 1 showed the uniaxial stress-strain curves. In a typical neutron diffraction experiment grains within $\pm 0.5^\circ$ from the scattering vector contribute to the registered intensity. However, in order to improve upon the statistical quality of the data we here average over $\pm 5^\circ$ in our presentation of numerical results. We assume that this increased tolerance does not have any major effect on the results other than to improve the statistical quality.

The lattice strains have been calculated for all crystallographic planes with Miller indices up to $\{531\}$, which is the unsymmetrical f.c.c. reflection with the lowest indices (we ignore lattice planes corresponding to forbidden reflections in the f.c.c. lattice, higher-order lattice reflections and reflections composed of two families of lattice planes). We only quote results for the lattice planes listed in Table 3 (in order to limit the number we have excluded the 420- and 422 reflections). Table 3 also gives the crystallographic multiplicities of the lattice planes, which is a factor of practical importance, since the intensity of a specific hkl reflection in a powder diffraction experiment is proportional to the multiplicity. The lattice strains in the different families of grains (the different reflections) in the respective directions are calculated from the stress tensor, provided by the polycrystal model, and the single crystal compliance tensor.

5. LATTICE STRAIN RESULTS

The results of the calculations are presented in five subsections: Section 5.1, the elastic Kröner stiffness of the reflections; Section 5.2, the elastic lattice strains vs the applied load; Sections 5.3 and 5.4, the standard deviation and the deviation from linearity in Section 5.2; Section 5.5, the residual lattice strain after unloading from different strains. For Sections 5.4 and 5.5 the results are presented in the conventional way with the independent variable (the plastic strain) along the x -axis and the results along the y -axis. For Sections 5.2 and 5.3 the results are presented differently — with the independent variable (the applied stress) along the y -axis and the results (the elastic lattice strain and their standard deviations) along the x -axis — in order to approach the presentation in a conventional stress-strain curve.

Table 3. The reflections considered their multiplicities

hkl	111	200	220	311	331	531
Multiplicity	8	6	12	24	24	48

The results are evaluated in terms of the advantages associated with hkl reflections showing a linear relation between the measured lattice strains and the actual state of macroscopic stress. In this connection it is relevant to remember the difference in elastic anisotropy of the three materials dealt with as expressed by $2C_{44}/(C_{11}-C_{12})$; for aluminum it is 1.22, for copper it is 3.21, and for austenitic steel it is 3.77 (for details see Table 1).

5.1. Diffraction elastic constants

There are great differences in the degree of elastic anisotropy in the materials dealt with in the present work, and this has a direct impact on the lattice strain levels observed in different orientations. At the grain size scale we have illustrated the orientation dependence of the elastic modulus for aluminum and copper in Fig. 6. The figure shows the normalized modulus with respect to the maximum value, which is found at the $\langle 111 \rangle$ orientation in cubic materials.

The trend in the orientation dependency of the modulus is identical for all f.c.c. materials, however, the numerical levels are dictated by the degree of elastic anisotropy. The variation in copper is much more pronounced than in aluminum, as shown in Fig. 6, where it is noticed that the minimum values are 0.86 and 0.41 for aluminum and copper, respectively.

Figure 6 dealt with the stiffness on a grain size scale, however, for practical utilization of neutron diffraction for stress/strain characterization we utilize the so-called diffraction elastic constants (DEC). In the present model these constants are determined as the average Kröner stiffness [18], and Table 4 shows the numerical values for the reflections considered here. Relative to the single crystal stiffness we observed the general trend that the reflections which are much stiffer (e.g. $\langle 111 \rangle$) or much more compliant (e.g. $\langle 200 \rangle$) than the macroscopic modulus are calculated to be less extreme.

5.2. Lattice strain development

Figures 7 and 8 show the relation between the applied stress and the elastic lattice strains parallel to and perpendicular to the tensile axis for the six reflections in the three materials. The lattice strain for a given reflection is determined by the stress state in the corresponding grains. Load redistribution between the grains therefore leads to changes in the lattice strains.

Table 4. The diffraction elastic constants of specific reflections (in GPa)

	E_{111}	E_{200}	E_{220}	E_{311}	E_{331}	E_{531}
Aluminum	73.3	67.8	71.8	70.2	72.3	71.2
Copper	158.0	101.5	138.7	121.8	143.8	131.2
Stainless steel	246.2	149.8	212.0	183.2	220.9	199.2

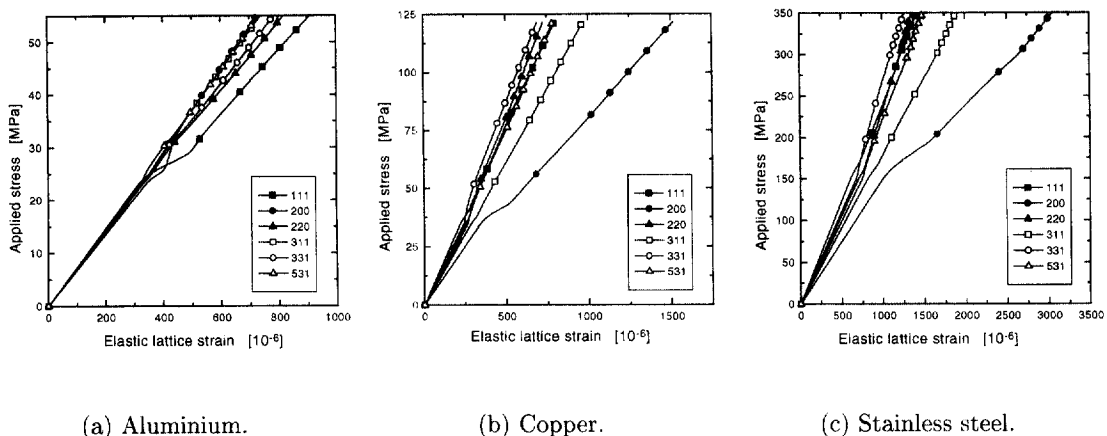


Fig. 7. Stress–strain response parallel to the tensile axis, here given for six reflections.

As seen in Fig. 7, the degree of redistribution of the load between the reflections (between the differently oriented grains) at the onset of plastic deformation increases as the elastic anisotropy increases, aluminum having the weakest elastic anisotropy and stainless steel the strongest. One should note the scale difference in the figures. This redistribution of the load is obviously determined by a combination of the elastic and the plastic anisotropy of the material.

The strain redistribution is quite similar in stainless steel and copper. Parallel to the tensile axis, Fig. 7, the two elastically softest reflections, 200 and 311, remain the softest in the plastic region, and the 331 and 220 reflections become the stiffest. Perpendicular to the tensile axis, Fig. 8, the 200 reflection experiences the largest redistribution in lattice strain and becomes the stiffest direction.

In aluminum, the strain redistribution is different from that in the other two materials. Parallel to the tensile axis the elastically stiffest reflection, 111, experiences the highest strain in the plastic region for a given applied load as it becomes the softest reflection in the plastic region, and the elastically softest reflection, 200, becomes one of the stiffest in the

plastic region. Perpendicular to the tensile axis, the redistribution is almost the same as the 111 reflection becomes the softest reflection in the plastic region and the 200 reflection becomes the stiffest. The differences in lattice strain in aluminum are rather small compared with the strain resolution in a neutron diffraction measurement ($\pm 50 \times 10^{-6}$), which would make them difficult to observe experimentally.

The redistribution of the lattice strains perpendicular to the tensile axis at the onset of plastic deformation is particularly dramatic for the 200 reflection. The lattice strain may even decrease with increasing applied stress. In order to understand this one must realize that the sub-set of grains with $\langle 200 \rangle$ perpendicular to the tensile axis (or for that matter any sub-set of grains with $\langle hkl \rangle$ perpendicular to the tensile axis) is composed of sub-sub-sets of grains with different orientations relative to the tensile axis. The sub-sub-sets actually have the tensile axis distributed along the $\langle 100 \rangle$ - $\langle 110 \rangle$ side of the unit triangle. A close investigation of the grains in these sub-sub-sets (with the exception of those close to $\langle 100 \rangle$) in terms of the numbers of active slip systems and the m -factors as quoted in Section

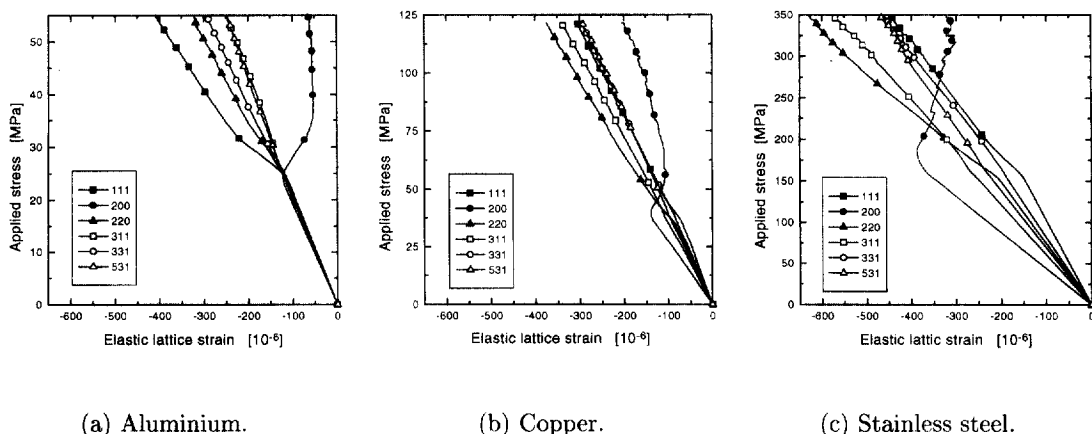


Fig. 8. Stress–strain response perpendicular to the tensile axis, here given for six reflections.

Table 5. Normalized stress parallel to the tensile axis for the different reflections

hkl	Aluminum	Copper	Steel	Taylor	Sachs
111	1.20	1.21	1.18	1.20	1.35
200	0.88	0.88	0.87	0.80	0.99
220	1.10	1.11	1.13	1.20	0.96
311	0.97	0.97	0.97	0.94	0.97
331	1.07	1.07	1.07	1.13	0.99
531	0.99	0.99	1.00	1.03	0.90

3 shows that their plastic contraction (perpendicular to the tensile axis) is much larger in the $\langle 100 \rangle$ direction than in the direction perpendicular to $\langle 100 \rangle$ (we are not giving the details, but it is relatively easy for the interested reader to check it). This means that the plastic contraction in the $\langle 100 \rangle$ direction is much larger than the contraction in the continuum matrix, which will introduce a tensile stress in the $\langle 100 \rangle$ direction counteracting the Poisson contraction and thereby introduce the dramatic change in the development of the lattice strain for the 200 reflection at the onset of plastic deformation. "Curling" is a well known experimental manifestation of the special behavior in the direction perpendicular to the tensile (or compression) axis in grains subjected to tension or compression in the $\langle 110 \rangle$ direction, e.g. [19].

As pointed out, Figs 7 and 8 reveal rather big differences between the three materials. And it is clear that the differences in elastic anisotropy, elastic constants and strength must be reflected in the results. In Table 5 we go behind these "trivial" (but of course very relevant) differences. The table gives the (average) normal stresses in the tensile direction divided by the applied stress for the different grain orientations in the three materials at specific applied stresses (all corresponding to 5% strain). These normalized stresses reflect the underlying polycrystal deformation pattern. They are almost identical in the three materials which agrees with the findings in Section 3, that the deformation pattern is basically the same in aluminum and copper. For comparison

the table also gives the normalized stresses for the Taylor and the Sachs model, calculated as the m -factor in the specific directions divided by the average m -factor. Again there is perfect agreement with the findings in Section 3: the deformation pattern derived from the self-consistent model is approximately half-way between those derived from the Taylor and the Sachs models.

5.3. Lattice strain variations

When we focus on specific sub-sets of grains having a specific lattice plane normal in a direction parallel to the tensile axis, all grains in this family will show nearly the same elastic lattice strain since the deformation is rotationally symmetric. When we focus on specific sub-sets of grains having a specific lattice plane normal in a direction perpendicular to the tensile axis, the elastic lattice strain will show great variations: a rotation around an axis perpendicular to the tensile axis changes the orientation relative to the tensile axis, and thereby the stress and strain state in the grains (e.g. Section 5.2). Figures 9 and 10 present the standard deviation of the elastic lattice strains within the different grain sub-sets.

Parallel to the tensile axis, the standard deviation is less than 10% of the measured lattice strains, see Figs 7 and 9. Perpendicular to the tensile axis, the standard deviations are much larger. For the 200 reflection in the plastic region the standard deviation is even larger than the average elastic lattice strain, see Figs 8 and 10. This particularly large standard deviation for the 200 reflection perpendicular to the tensile axis is due to the special behavior of the grain sub-sub-sets involved as described in Section 5.2.

5.4. Deviation from linearity

In Section 5.2 we observed a high degree of non-linearity in the lattice strain response, and we observed great differences between the longitudinal and the transverse lattice strain response. In view of

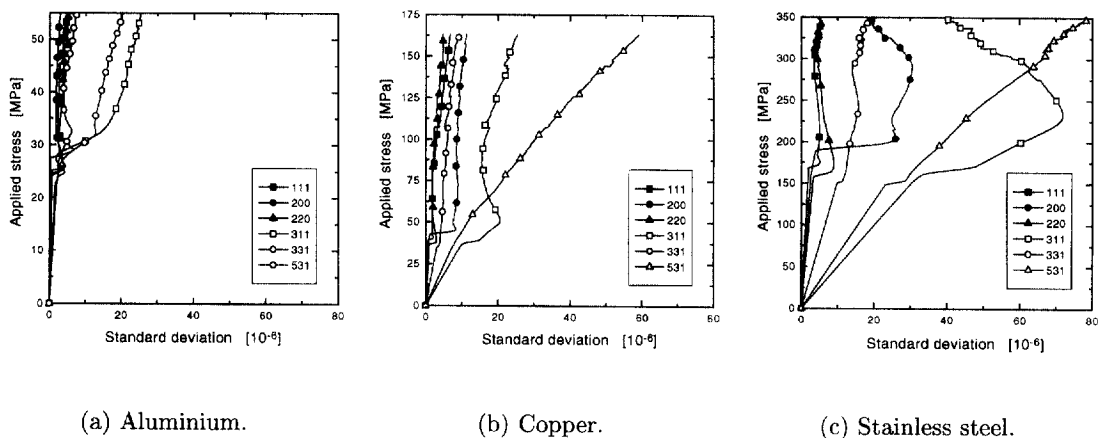


Fig. 9. Standard deviation of the elastic lattice strains parallel to the tensile axis.

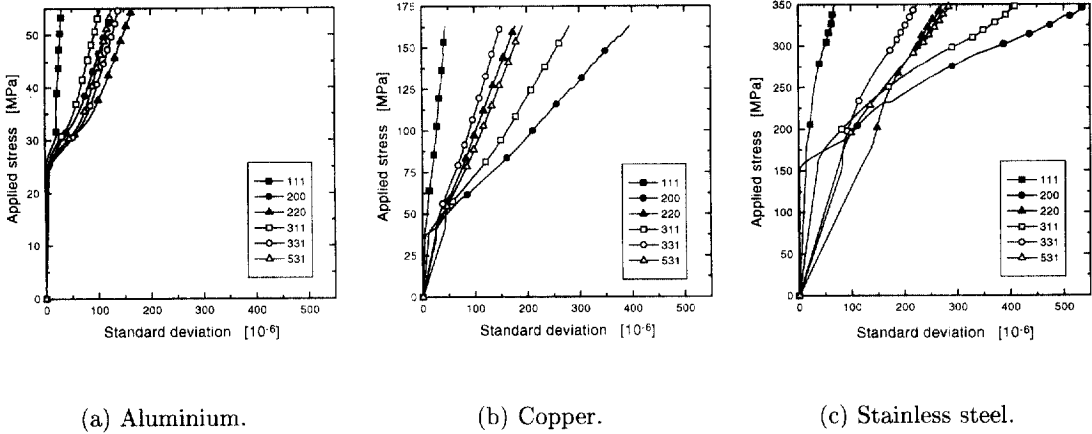


Fig. 10. Standard deviation of the elastic lattice strains perpendicular to the tensile axis.

the importance of linearity as a criterion for the selection of the most suitable reflection(s) we have extracted the deviation from linearity in the plastic region parallel to and perpendicular to the tensile axis from Figs 7 and 8 (defined as the, positive or negative, deviation along the lattice-strain axis from the extrapolated elastic line for the reflection in question). In Figs 11 and 12 the results are plotted vs plastic strain (obtained from the applied stresses in Figs 7 and 8 via the stress-strain curves in Fig. 1).

Parallel to the tensile axis the aluminum results are quite different from the copper and the stainless-steel results (which are quite similar). The 200 reflection, for instance, has a negative deviation in aluminum and a positive deviation in copper and stainless steel. The magnitude of the deviations relative to the actual lattice strains is also clearly smaller in aluminum than in the other two materials. This demonstrates the dominant effect of elastic anisotropy. Perpendicular to the tensile axis the aluminum results are not very different from the results for the other two materials, neither in sign nor in relative magnitude.

5.5. Residual lattice strains

In Sections 5.2, 5.3 and 5.4 we have presented the lattice strain response for the different *hkl* reflections under tensile loading, starting at zero for no load. However, after loading into the plastic regime one may return to a situation with zero macroscopic stress, but now not necessarily with zero lattice strains — because of the non-linear behavior of the lattice strains in the plastic regime. It is obviously important to know the different lattice strains after unloading, the residual lattice strains. Therefore, we have made calculations with loading to various plastic strains followed by unloading.

It turns out that the results are practically identical to the results in Figs 11 and 12 for the deviation from linearity (but now the *x*-axis gives the plastic strains at which unloading takes place, and the *y*-axis gives the residual lattice strains). The reason why the residual lattice strains are practically identical to the deviations from linearity is that there is no slip during unloading. This is not as trivial as it may seem; using a Kröner-type [8] self-consistent model Leffers and Pedersen [20] did observe slip during unloading (with a significant effect on the re-

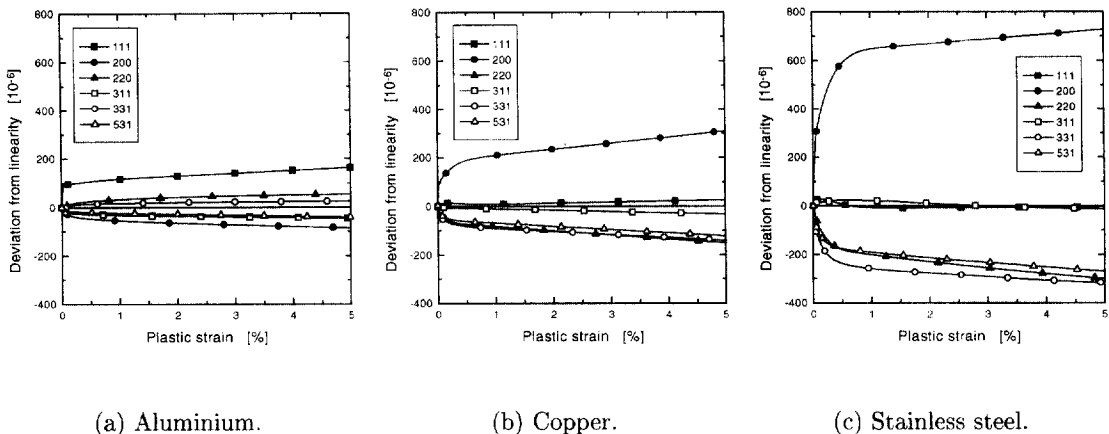


Fig. 11. Elastic strain deviation from linearity parallel to the tensile axis.

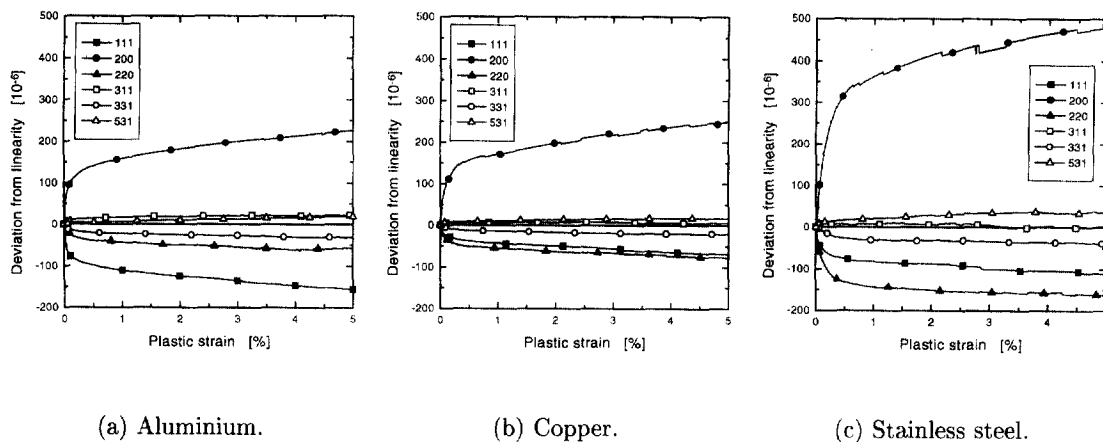


Fig. 12. Elastic strain deviation from linearity perpendicular to the tensile axis.

sidual stresses and the residual lattice strains). Without slip during unloading there is only one reason for a (small) difference between the residual lattice strains and the deviations from linearity, *viz.* the development of a weak texture during plastic straining: the deviations are obtained by extrapolating the elastic responses in a texture-free material whereas the residual strains are obtained by elastic unloading of a material with a weak texture.

6. DISCUSSION

The present investigation is not the first time self-consistent modelling (or other polycrystal modelling) has been used in connection with diffraction measurements of internal stresses. With reference to neutron diffraction we may quote MacEwen *et al.* [21], Leffers and Lorentzen [22] and Tomé *et al.* [23]; with reference to X-ray diffraction we may quote Krier *et al.* [24]. However, the present work specifically addresses the effect of elastic anisotropy and includes a systematic theoretical investigation of the interplay between type-1 and type-2 stresses and its bearings on the practical utilization of the neutron diffraction technique for stress/strain characterization.

For the texture-free (or almost texture-free) materials investigated in the present work, Hutchinson's self-consistent model leads to a "universal" deformation pattern, independent of elastic anisotropy and strength parameters (apart from the very early stage of plastic deformation). We do not believe that the specific selection of Hutchinson's model is very important. Any self-consistent model with soft interaction with the continuum matrix, e.g. the models of Molinari *et al.* [9] and Lebensohn and Tomé [10], would probably lead to very much the same results. However, when the deformation pattern is translated into lattice strains, elastic anisotropy and strength parameters play decisive roles. We are convinced that such self-consistent models are better than simpler models like the Sachs and

the Taylor models. There is no physical reason why the individual grains should interact with a continuum matrix with properties which are different from those of the average grain (the Taylor model correspond to an infinitely strong matrix and the Sachs model correspond to a very weak matrix). The only obvious shortcoming of the self-consistent model is that it is a 1-site model [9], i.e. that the individual grain interacts with a continuum matrix and not with specific neighboring grains.

The results of the numerical simulations are to be checked experimentally in subsequent publications (we do quote results from one of these). However, we do here draw a number of conclusions already on the basis on the model calculations.

6.1. hkl selection for stress/strain characterization

The ideal reflection will have a linear response parallel to and perpendicular to the tensile axis and hence zero residual lattice strain after unloading. The 311 reflection comes quite close to this ideal for all three materials. In the range up to 5% plastic strain the deviation from linearity of the 311 reflection is well within the normal standard deviation in a neutron diffraction experiment which is about $\pm 50 \times 10^{-6}$. The 311 reflection has the further advantage that it is rather insensitive to the model selected: as shown in Table 5 we obtain approximately the same result for the present model, the upper-bound Taylor model and the (realistic) lower-bound Sachs model [25]. Because of the approximately linear response one may for the 311 reflection simply extrapolate the Kröner diffraction elastic constants into the plastic regime.

One frequently sees references to a rule of thumb that one just has to use a high-index (or low-symmetry) reflection. The present results do not support this rule of thumb: the 331 reflection with the same symmetry as the 311 reflection and the 531 reflection with a lower symmetry shows a greater deviation from linearity than the 311 reflection.

The selection of non-linear reflections which do have a strong recollection of the plastic deformation history and hence carries extensive levels of residual intergranular stresses, would make appropriate interpretation of diffraction results complicated. Take for instance the results for stainless steel samples which have been unloaded after 1% plastic strain. Parallel to the tensile axis the 200 reflection shows a residual tensile lattice strain of $\sim 650 \times 10^{-6}$ (Fig. 11(c)). In case this reflection is selected as our probe for macroscopic internal stresses and the lattice strain was converted to stress following our findings for the relation between the macroscopic stress and the deviation in lattice spacing (see Fig. 7(c)) this would give a stress of ~ 90 MPa in contradiction with the obvious macroscopic stress level of zero in the unloaded specimen.

6.2. Other conditions

It should be underlined that all the calculations refer to tensile deformation of texture-free materials, and hence the specific results are only relevant for these conditions (the results would of course also apply to compression of texture-free materials after a change of sign). For other deformation modes and for textured materials new calculations should be made. It is obvious, for instance, that for tensile deformation of a material with a very strong $\langle 111 \rangle$ fiber texture the 111 reflection (and not the 311 reflection) will have a linear response parallel to the tensile axis.

6.3. Experimental evaluation of model predictions

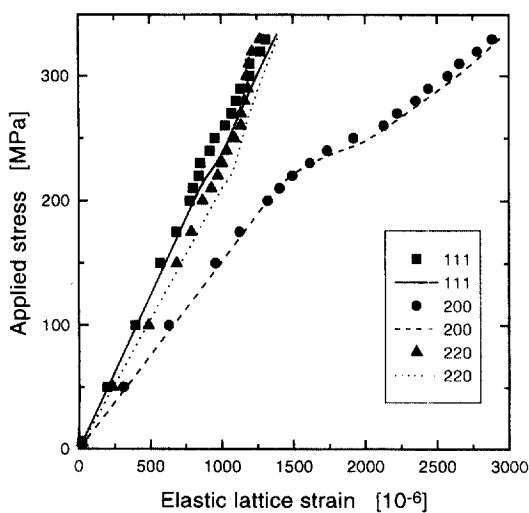
The aim of the present work is to present the results of the model calculations. However, in order

to establish a certain experimental basis, we shall present some preliminary results from an experimental investigation where lattice strains parallel to the tensile axis for the different reflections have been measured by neutron diffraction during *in-situ* tensile loading of stainless steel specimens. The measured lattice strains are shown in Fig. 13 together with the theoretical stress/lattice-strain curves. The theoretical curves deviate somewhat from those in Fig. 7(c) because they refer to the actual specimens with some initial texture.

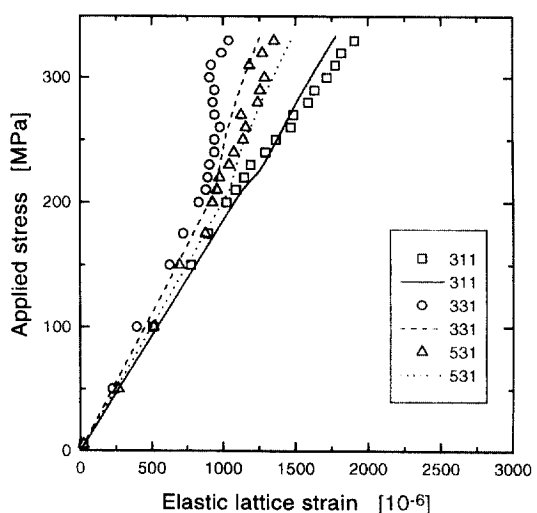
The basic difference between the theoretical curves for the different reflections is reproduced very well by the experimental data throughout the deformation range considered here. A detailed discussion and comparison between model prediction and diffraction results is to appear in a subsequent publication by Clausen *et al.* [26]. However, we do want to make two statements:

(i) The 311 reflection shows an approximately linear response even though it is not as perfectly linear as in Fig. 7(c).

(ii) The experiments reproduce the theoretical relation between the 111 and 220 reflections. This refers to the largest deviation of the self-consistent deformation pattern from that of the Taylor model as shown in Fig. 4. It is obviously correct that the *m*-factor in the vicinity of $\langle 110 \rangle$ is much smaller than that in the vicinity of $\langle 111 \rangle$ as predicted by the self-consistent model. Identical *m*-factors for $\langle 110 \rangle$ and $\langle 111 \rangle$, as predicted by the Taylor model, would lead to a much larger difference between the 111 and 220 reflections in Fig. 13 (corresponding to the large difference in effective Young's modulus), e.g. Table 4.



(a) 111, 200 and 220 reflections.



(b) 311, 331 and 531 reflections.

Fig. 13. Calculated (lines) and measured (symbols) stress-strain response parallel to the tensile axis for stainless steel.

7. CONCLUSION

We have presented numerical results from a self-consistent modelling scheme for polycrystal deformation with specific emphasis on the elastic and plastic anisotropy. The data presented are relevant to both scientific and engineering utilization of neutron diffraction techniques for the characterization of residual stresses. Through calculations for three different f.c.c. materials exhibiting different degrees of elastic anisotropy we have quantified the *hkl* dependence of the lattice strain response to uniaxial loading. For aluminum the variations are in the observable range even though the numerical scale is small with the largest difference, observed between the 111 and the 200 reflection, not exceeding $\sim 2 \times 10^{-4}$ at the maximum load considered (55 MPa). For the highly anisotropic (and stronger) stainless steel the numerical scale is much larger with the largest difference, observed between the 200 and the 311 reflections, amounting to $\sim 1750 \times 10^{-6}$ at the maximum load considered (350 MPa). The numerical results show a high degree of non-linearity in the plastic regime, producing residual intergranular strains upon unloading. Certain *hkl* reflections, however, continue to show an approximately linear lattice strain response far into the plastic regime and unload linearly to a state of zero residual intergranular strain. Such *hkl* reflections have little recollection of the plastic deformation history, and they would be the best choice for a specific *hkl* reflection to serve as the internal probe for macroscopic residual stresses and strains. In texture-free materials the 311 reflection is particularly well suited for this purpose, while other reflections with an identical or lower symmetry, like the 331 or the 531 reflection, respectively, are less perfect.

Acknowledgements—We thank J. Christoffersen, The Technical University of Denmark, J. W. Hutchinson, Harvard University and N. Hansen, Risø National Laboratory for helpful discussions. The work was carried out within the Engineering Science Centre for Structural Characterization and Modelling of Materials at Risø National Laboratory.

REFERENCES

1. Macherauch, E. and Kloos, K. H., in *Proc. 1st Int. Conf. on Residual Stresses*, ed. E. Macherauch and V. Hauk, 1986, p. 3.
2. Sachs, Z., *Ver. Dtsch. Ing.*, 1928, **72**, 734.
3. Taylor, G. I., *J. Inst. Metals*, 1938, **62**, 307.
4. Bishop, J. W. F. and Hill, R., *Phil. Mag.*, 1951, **42**, 414.
5. Bishop, J. W. F. and Hill, R., *Phil. Mag.*, 1951, **42**, 1298.
6. Bishop, J. W. F., *Phil. Mag.*, 1953, **44**, 51.
7. Hutchinson, J. W., *Proc. R. Soc. London A*, 1970, **319**, 247.
8. Kröner, E., *Acta metall.*, 1961, **9**, 155.
9. Molinari, A., Canova, G. R. and Ahzi, S., *Acta metall.*, 1987, **35**, 2983.
10. Lebensohn, R. A. and Tomé, C. N., *Acta metall. mater.*, 1993, **41**, 2611.
11. Clausen, B. and Lorentzen, T., Risø-R-970(EN), Risø National Laboratory, DK-4000 Roskilde, Denmark, 1997.
12. Clausen, B. and Lorentzen, T., *Met. Trans A*, 1997, in press.
13. Hill, R., *J. Mech. Phys. Solids*, 1966, **14**, 95.
14. Dieter, G. E., *Mechanical Metallurgy*. McGraw-Hill, 1988.
15. Ledbetter, H. M., *Physica status solidi (a)*, 1984, **A85**, 89.
16. Bunge, H.-J., *Texture Analysis in Materials Science*. Butterworth and Co, 1982.
17. Clausen, B., Thesis, Risø-R-985(EN), Risø National Laboratory, DK-4000 Roskilde, Denmark, 1997.
18. Kröner, E., *Z. phys.*, 1958, **151**, 504.
19. Hosford, W. F., *Trans. Met. Soc. AIME*, 1964, **230**, 12.
20. Leffers, T. and Pedersen, O. B., unpublished work.
21. MacEwen, S. R., Christodoulou, N., Tomé, C., Jackman, J., Holden, T. M., Faber, J. and Hitterman, R. L., *Proceedings ICOTOM*, Vol. 8, ed. J. S. Kallend and G. Gottstein. The Metallurgical Society, Warrendale, 1988, p. 825.
22. Leffers, T. and Lorentzen, T., *Measurement of Residual and Applied Stress Using Neutron Diffraction*, ed. M. T. Hutchings and A. D. Krawitz, Kluwer Academic Publishers, Dordrecht, 1992, p. 171.
23. Tomé, C. N., Christodoulou, N., Holt, R., Woo, C. H., Lebensohn, R. A. and Turner, P. A., *Proc. 15th Int. Risø Symposium on Materials Science*, ed. S. I. Andersen *et al.* Risø National Laboratory, Roskilde, 1994, p. 169.
24. Krier, J., Ruppertsberg, H., Berveiller, M. and Lipinski, P., *Textures Microstruct.*, 1991, **14-18**, 1147.
25. Leffers, T., *Physica status solidi (a)*, 1995, **149**, 69.
26. Clausen, B., Lorentzen, T., Bourke, M. A. M. and Daymond, M. R., *Mater. Sci. Engng*, December 1997, submitted.